Insights into Imaging
ESR EUROPEAN SOCIETY OF RADIOLOGY

ORIGINAL ARTICLE

Open Access

A feasibility study of reduced full-of-view synthetic high-*b*-value diffusion-weighted imaging in uterine tumors

Qian Tang[1,2], Qiqi Zhou[1], Wen Chen[1], Ling Sang[1], Yu Xing[1], Chao Liu[1], Kejun Wang[1], Weiyin Vivian Liu[3*] and Lin Xu[1*]

Abstract

Objectives This study aimed to evaluate the feasibility of reduced full-of-view synthetic high-*b* value diffusion-weighted images (rFOV-syDWIs) in the clinical application of cervical cancer based on image quality and diagnostic efficacy.

Methods We retrospectively evaluated the data of 35 patients with cervical cancer and 35 healthy volunteers from May to November 2021. All patients and volunteers underwent rFOV-DWI scans, including a 13b-protocol: $b = 0$, 25, 50, 75, 100, 150, 200, 400, 600, 800, 1000, 1200, and 1500 s/mm^2 and a 5b-protocol: $b = 0$, 100, 400, 800,1500 s/mm^2. rFOV-syDWIs with *b* values of 1200 (rFOV-syDWI$_{b=1200}$) and 1500 (rFOV-syDWI$_{b=1500}$) were generated from two different multiple-b-value image datasets using a mono-exponential fitting algorithm. According to homoscedasticity and normality assessed by the Levene's test and Shapiro–Wilk test, the inter-modality differences of quantitative measurements were, respectively, examined by Wilcoxon signed-rank test or paired t test and the inter-group differences of ADC values were examined by independent t test or Mann–Whitney U test.

Results A higher inter-reader agreement between SNRs and CNRs was found in 13b-protocol and 5b-protocol rFOV-syDWI$_{b=1200/1500}$ compared to 13b-protocol rFOV-sDWI$_{b=1200/1500}$ ($p < 0.05$). AUC of 5b-protocol syADC$_{mean,b=1200/1500}$ and syADC$_{minimum,b=1200/1500}$ was equal or higher than that of 13b-protocol sADC$_{mean,b=1200/1500}$ and sADC$_{minimum,b=1200/1500}$.

Conclusions rFOV-syDWIs provide better lesion clarity and higher image quality than rFOV-sDWIs. 5b-protocol rFOV-syDWIs shorten scan time, and synthetic ADCs offer reliable diagnosis value as scanned 13b-protocol DWIs.

Key points

- rFOV-syDWI provided better lesion clarity and image quality while shortening scan time.
- Scanned and synthetic ADCs have the same diagnostic value for cervical cancer.
- Scanned and synthetic ADC$_{mean,\ minimum}$ can distinguish cervical lesions from normal tissue

*Correspondence:
Weiyin Vivian Liu
weiyin.liu@qq.com
Lin Xu
xulinst@sohu.com
Full list of author information is available at the end of the article

Keywords Cervical cancer, Reduced field-of-view diffusion-weighted imaging, Synthetic diffusion-weighted image, Magnetic resonance image

Introduction

Diffusion-weighted imaging (DWI) is an essential functional imaging technology for noninvasively detecting diffusion movement orientation and local restriction degree of water molecules in living tissues, thus indirectly reflecting the changes in tissue microstructure [1]. It can provide both good visual clarity of tumors with high signal intensity and quantitative information like apparent diffusion coefficient (ADC), so a widely used single-shot echo-planar imaging (EPI) DWI is applied to the diagnosis and treatment of various diseases including gynecological tumors [2]. Previous studies have shown that ADC value can be used to differentiate cervical cancer from normal cervix tissues and predict the stage and type of cervical cancer [3, 4]. DWI can also effectively assess the invasion depth of the uterine corpus and infiltration range of parauterine organ by cervical cancer. Therefore, DWI is of importance for the evaluation and treatment of uterine tumors.

Currently, the most commonly used diffusion-weighted imaging (DWI) is used in either clinical diagnosis or scientific research of uterine diseases using single-shot k-space trajectory echo-planar imaging (SS-EPI). However, SS-EPI DWI is prone to have image distortion, blurring, and signal loss due to its narrow bandwidth in the phase coding direction and long readout time [5, 6]. In recent years, DWI with reduced field-of-view (r-FOV) in the phase-encoding direction has been developed to overcome magnetic susceptibility and motion artifacts [7] that occur in full field-of-view (f-FOV) acquisition including signals from liquid, gas, and other substances other than target tissues [7, 8]. rFOV-DWI reduces the number of phase-encoding lines and readout time via selective RF excitation pulse in collocation with frequency encoding gradient and increases echo signal intensity using the 180° refocusing pulse [9, 10], eventually improving image quality with higher image resolution, less magnetic sensitivity and motion artifact. Up to date, it has been in particular applied to spinal cord imaging, pancreatic lesions, and cervical cancer [7, 11, 12].

Another challenge of DWI applications in human body is the selection of diffusion sensitive factors (*b* values). Currently, *b* values used for disease evaluation in most in vivo DWI studies usually range between 0 and 1000 s/mm^2 [13], and *b* values greater than 1000 s/mm^2 are widely used in prostate, brain, and breast diseases [13–15]. High-b-value DWI reduces the T2 throughout effect, resulting in a higher contrast between lesions and surrounding tissues and achieving better tumor detection, especially for small lesions and abdominal hollow organ tumors [16, 17]. Background signals on high-b-value DWIs in the diagnosis of cervical cancers, intestines, and bladders showed more significantly suppressed than those in the relatively low *b* value ($b=800$ s/mm^2) and better efficacy of lesion detection. Decidualized endometrioma on DWIs with a *b* value of 1500 s/mm^2 could be distinguished from ovarian cancer more easily via visual observation [18]. Although high-b-value DWI has been widely applied in clinical practices, it is challenging to obtain several high-*b*-value images for the reasons of prolonged echo time, relatively long scan time and more eddy distortion as *b* value and acquisition time increased, leading to patient discomfort, increased motion artifacts and decreased signal-to-noise ratio (SNR) [16, 19, 20]. Thus, high-b-value DWI is limited in the clinical applications.

Synthetic DWIs (syDWIs) are calculated from a group of scanned DWIs with different *b* values by extrapolating the fitted signal attenuation curve [21, 22]. SyDWIs with high *b* values showed better SNR and less image distortion than scanned high-*b*-value DWIs. They also showed a higher contrast-to-noise ratio (CNR) between the lesions and the background compared to low-*b*-value DWIs, improving the efficiency of lesion detection in research of systemic malignant tumors, prostate cancer, breast cancer, and liver metastasis [5, 23–25]. SyDWI with $b=1500$ s/mm^2 had higher image quality and detection rate in the diagnosis of pancreatic cancer than the real scanned DWIs with a high *b* value. Only one application of high-*b*-value syDWIs on 1.5 T demonstrated that the significance of liver metastases and detection rate were higher than the scanned ones.

Normally, two to five *b* values were set in one DWI to generate more reliable synthetic high-*b*-value DW images in the diagnosis of liver metastases [26], Crohn's disease [27], prostate [14], and pancreas [11]. In addition, the combination of small field weighted imaging and synthetic high-*b*-value diffusion-weighted imaging has been applied in pancreatic tumors [11] for improving detection efficiency. But there was no computed high-*b*-value uterus DW study to assure 5b-protocol DWI could be used in clinical diagnosis. Therefore, the feasibility and reliability of 5b-protocol DWI-generated high-*b*-value rFOV-syDWIs and rFOV-ADCs in clinical diagnosis of cervical disease should be examined using 13b-protocol DWI-generated scanned and synthetic DW images as a

standard reference to compare image quality and diagnostic efficiency including lesion clarity and contrast between lesion and parenchyma.

Materials and methods

Patients

This study was approved by the institutional review board (IRB:2022KS013) of our hospital. A total of 35 patients with cervical cancer and 35 healthy volunteers who visited our hospital from May to November 2021 were prospectively recruited in this study and received clinicians' diagnosis based on the Federation of Gynecology and Obstetrics (FIGO, 2019) [28]. All gave signed written informed consent. Inclusion criteria were as follows: (1) no contraindications to MRI scans or prior therapy; (2) no uncontrollable comorbidities or malignant tumors; (3) receiving MRI scans including a rFOV-DWI sequence; (4) good image quality without artifacts; (5) clinicopathological data were complete; and (6) the maximum diameter of the lesion was > 1 cm and the lesion can be accurately delineated (only for patients). Details are shown in Fig. 1.

Magnetic resonance imaging and postprocessing

rFOV-DWI was acquired with TR/TE/ = 4000/71.6 ms, field of view = 20 × 20 cm^2, matrix = 110 × 90, layer thickness = 4 mm, no gap on 1.5 Tesla (SIGNA Voyager, GE Healthcare). Two multiple-b-value protocols were used: (1) a 13b-protocol as a standard reference: $b = 0$, 25, 50, 75, 100, 150, 200, 400, 600, 800, 1000, 1200, and 1500 s/mm^2; (2) a 5b-protocol as our proposal: $b = 0$, 100, 400, 800,1500 s/mm^2 with NEX = 1 and 2 for b less and more than 200 s/mm^2, respectively, for a total scan time of 11 min and 12 s as well as 4 min. Noteworthily, scan time depends on the number of used b values; meanwhile, rFOV-DWI alone elevates lesion conspicuity and edge delineation. 13b-protocol was chosen as a standard reference due to more accurate ADC maps using a mono- or bi-exponential computation model when more used b values are used and showing good diagnosis efficiency in cervical cancer [1, 29–32]. Each subject was instructed to properly empty the bladder to reduce artifacts of intestinal peristalsis and urine electrolyte around 30 min before scanning. All patients were free-breathing and placed in the supine position with an 8-channel phased coil over the abdomen. The top and bottom of scan coverage were positioned at the anterior and superior iliac spine and the lower margin of the symphysis pubis to include the entire uterus. rFOV-syDWIs with b values of 1200 (rFOV-syDWI$_{b=1200}$) and 1500 (rFOV-syDWI$_{b=1500}$) were automatically generated from 5b-protocol and 13b-protocol image datasets by an inline mono-exponential fitting algorithm on 1.5 T MRI console without labor consumption. Then, all 5b-protocol and 13b-protocol scanned and synthetic DW images were transferred to image postprocessing workstation (GE Advanced Workstation 4.7) and both rFOV-sADCs and rFOV-syADCs with b value of 1200 and 1500 s/mm^2 were computed.

Subjective image quality analysis

All image evaluation was performed by two radiologists with at least 10 years of experience in abdominal radiographic diagnosis. Image quality was rated on a four-point Likert scale with respect to the following four aspects (U1–U4). U1: overall image quality (4 = excellent image quality, 3 = good image quality, not affecting interpretation, 2 = fair image quality and somewhat affecting interpretation, 1 = poor image quality), U2: anatomic detail (4 = excellent delineation of anatomic structure with blurred margin, 3 = good delineation of anatomic structure with a sharp margin, 2 = fairly delineation of anatomic structure with blurred margin, 1 = poorly visualized anatomy), U3: lesion conspicuity (4 = lesions identified as distinct signal differences with a clear lesion margin, 3 = lesions identified as signal difference, 2 = lesions identified as slight signal differences, 1 = lesion not identified as signal is rough), U4: level of geometric deformation (4 = absent, 3 = mild, 2 = moderate, 1 = severe).

Objective image quality analysis

The same two radiologists double-blindly assessed rFOV-sDWIs and rFOV-syDWIs with b values of 1200 and 1500 s/mm^2. Measurements were obtained as follows: (1) average signal intensity of a lesion (S_{lesion}); (2) average signal intensity of gluteus maximus (S_{tissue}); and (3) standard deviation of signal intensity of subcutaneous fat ($SD_{background}$). The following formula is used to calculate the signal-to-noise ratio (SNR) and contrast-to-noise ratio (CNR) for DWI images:

$$SNR = \frac{S_{lesion}}{SD_{background}} \quad CNR = \frac{S_{lesion} - S_{tissue}}{\sqrt{S^2_{lesion} + SD^2_{tissue}}}$$

Quantitative assessment

Scanned and synthetic ADCs ($sADC_{b=1200/1500}$, $syADC_{b=1200/1500}$) were generated, respectively, based on rFOV-sDWIs and rFOV-syDWIs with two values of 0 and 1200 or 1500 on GE postprocessing workstation (GE Advanced Workstation 4.7). Two experienced radiologists double-blindly drew three ROIs with an area of 50 ± 5 mm on the images with the maximum lesion cross section for the patient group or maximum cervix cross-section for the healthy volunteers using T2W images as reference and placed in avoidance of

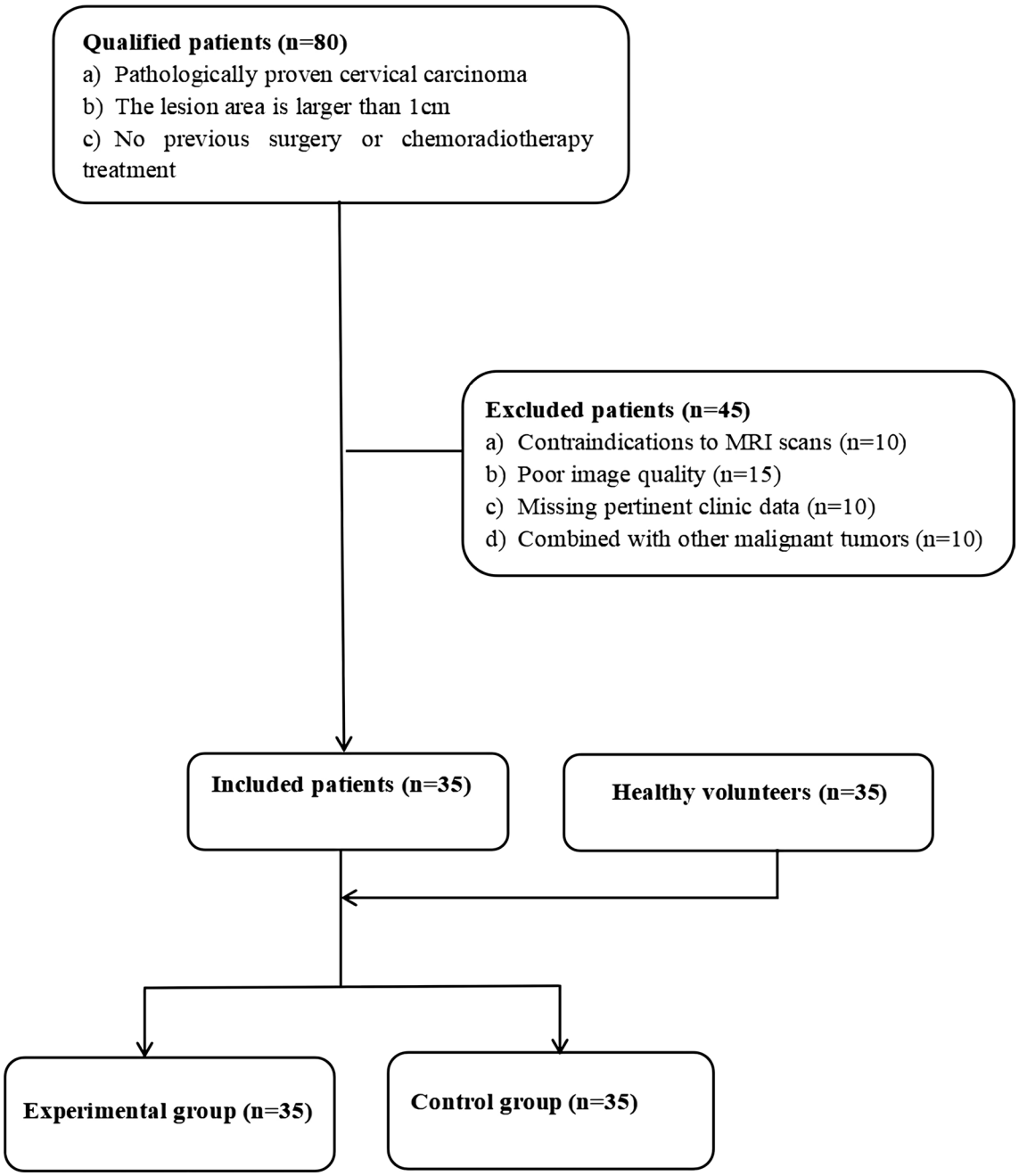

Fig. 1 Workflow of subject inclusion and exclusion in this study

visible blood vessel, tumors, hemorrhage, and necrosis. Histogram-derived parameters based on ADC values, including mean (ADC_{mean}), minimum ($ADC_{minimum}$), skewness ($ADC_{skewness}$), and kurtosis ($ADC_{kurtosis}$), of scanned and synthetic DWIs were then obtained.

Statistical analysis

SPSS26.0 (IBM, Armonk, NY) was used for statistical analysis. The inter-reader differences of qualitative measurements (U1-U4) on the actual scanned DWI and syDWI were analyzed by weighted kappa analysis: 0.2 ~ 0.4 poor consistency, 0.41 ~ 0.60 medium consistency, 0.61 ~ 0.80 good consistency, > 0.81 excellent consistency. The inter-modality differences of quantitative measurements (CNR, SNR, and ADC-related values) were, respectively, examined by Wilcoxon signed-rank test or paired t test according to homoscedasticity and normality, respectively, assessed by the Levene's test and

Table 1 Inter-rater agreements on subjective assessment of scanned and synthetic 13b-protocol rFOV-DWIs with *b* values of 1200 and 1500 s/mm^2

B value	Overall image quality				Anatomy				Lesion conspicuity				Geometric distortion			
	Reader1	Reader2	Kappa	*p* value	Reader1	Reader2	Kappa	*p* value	Reader1	Reader2	Kappa	*p* value	Reader1	Reader2	Kappa	*p* value
s_{13b}1200	1.58 ± 0.49	1.64 ± 0.48	**0.767****	***p* < 0.001**	1.64 ± 0.48	1.67 ± 0.47	**0.816****	***p* < 0.001**	1.61 ± 0.49	1.61 ± 0.49	**0.766****	***p* < 0.001**	1.61 ± 0.49	1.64 ± 0.48	**0.704****	***p* < 0.001**
sy_{13b}1200	3.53 ± 0.50	3.53 ± 0.50	**0.889****	***p* < 0.001**	3.53 ± 0.50	3.56 ± 0.50	**0.944****	***p* < 0.001**	3.53 ± 0.50	3.53 ± 0.50	**0.889****	***p* < 0.001**	3.50 ± 0.50	3.53 ± 0.50	**0.833****	***p* < 0.001**
s_{13b}1500	1.64 ± 0.48	1.64 ± 0.48	**0.759****	***p* < 0.001**	1.60 ± 0.49	1.64 ± 0.48	**0.822****	***p* < 0.001**	1.58 ± 0.48	1.58 ± 0.49	**0.771****	***p* < 0.001**	1.58 ± 0.49	1.68 ± 0.47	**0.706****	***p* < 0.001**
sy_{13b}1500	3.58 ± 0.49	3.58 ± 0.49	**0.886****	***p* < 0.001**	3.56 ± 0.50	3.59 ± 0.49	**0.943****	***p* < 0.001**	3.58 ± 0.49	3.58 ± 0.49	**0.886****	***p* < 0.001**	3.56 ± 0.50	3.58 ± 0.50	**0.830****	***p* < 0.001**

s = scanned DWI, sy = synthetic DWI, the image scores are expressed as means ± standard deviations, *p* values < 0.001 were considered statistically significant

**$p < 0.001$

Shapiro–Wilk test; the inter-group differences of ADC values were examined by independent t test or Mann–Whitney U test according to homoscedasticity and normality assessed by Levene's test and Shapiro–Wilk test. All data were expressed as mean (± SD). In addition, the area under ROC curve (AUC) was compared to test the differential performance of ADCs between cervical cancer patients and healthy volunteers. *P* values < 0.05 were considered indicative of statistical significance for all tests.

Results

Subjective and objective image quality scores

Image quality scores of rFOV-sDWI$_{b=1200/1500}$ and rFOV-syDWI$_{b=1200/1500}$ computed based on 5b- and 13b-protocols were evaluated by two radiologists (Tables1 and 2). For both multiple-b-value protocols, there were statistically higher scores (U1-U4) between scanned and synthetic DWIs ($p < 0.05$) and statistically higher inter-reader agreements on synthetic DWIs (κ for rFOV-syDWI$_{b=1200}$ and rFOV-syDWI$_{b=1500}$ computed with the 13b-protocol of: U1 = 0.889, 0.886, U2 = 0.944, 0.943, U3 = 0.889, 0.886, U4 = 0.833, 0.830; with the 5b-protocol of: U1 = 0.882, 0.885, U2 = 0.935, 0.936, U3 = 0.878, 0.885, U4 = 0.833,0.830) than scanned ones (κ for rFOV-sDWI$_{b=1200}$ and rFOV-sDWI$_{b=1500}$ computed with the 13-*b*-value protocol of: U1 = 0.767, 0.759, U2 = 0.816, 0.822, U3 = 0.766, 0.771, U4 = 0.704, 0.706) ($p < 0.001$).

Objective image quality values (SNR and CNR) measured on both rFOV-sDWIs and rFOV-syDWIs with a *b* value of 1200 and 1500 are shown in Fig. 2. SNRs of 13b-protocol rFOV-syDWI$_{b=1200/1500}$ (31.48 ± 7.44, 21.9 ± 6.01) and 5b-protocol ones (24.6 ± 6.01, 16.79 ± 4.43) were significantly higher than that of 13b-protocol rFOV-sDWI$_{b=1200/1500}$ (17.18 ± 3.95, 14.39 ± 3.52). CNRs of 13b-protocol rFOV-syDWI$_{b=1200/1500}$ (0.36 ± 0.11,0 0.33 ± 0.13) and 5b-protocol ones (0.36 ± 0.12, 0.31 ± 0.14) were also significantly higher than that of 13b-protocol rFOV-sDWI$_{b=1200/1500}$ (0.32 ± 0.12, 0.27 ± 0.12).

Quantitative assessment

Significant differences of histogram-derived ADC values in cervical cancer group were found between scanned and synthetic ADC values (Fig. 3a, b). For ADCs by 13b-protocol rFOV-syDWIs and rFOV-sDWIs, mean and minimum of syADC$_{b=1200/1500}$ were higher than those of sADC$_{b=1200/1500}$. For ADC computed by 5b- and 13b-protocol rFOV-syDWIs, there is no significant difference in histogram-derived parameters from both syADC$_{b=1200/1500}$ (Fig. 3c, d).

The AUCs of 13b-protocol syADC$_{mean}$ and syADC$_{minimum}$ were equal or higher than those of 13b-computed sADC$_{mean}$ and sADC$_{minimum}$ (Fig. 4a, b, Tables 3, 4). The AUCs of 5b-protocol syADC$_{mean}$ and syADC$_{minimum}$ were approximately equivalent to those of 13b-protocol syADC$_{mean}$ and syADC$_{minimum}$ (Fig. 4c, d, Tables 5, 6). The AUCs of other parameters are shown (Fig. 4, Tables 3, 4, 5, 6). Figure 5 illustrates the scanned and synthetic rFOV-DW images and a corresponding axial T2-weighted image of a patient with cervical cancer.

Discussion

This was the first study to explore the diagnostic value of uterine tumors based on synthetic high-b-value synthetic DWIs and also ADCs using the reduced field-of-view DWI sequence. We validated 5b-protocol DWI could be an optimal approach to generate high-b-value rFOV-DW images and corresponding ADC maps due to its equivalent diagnosis performance to 13b-protocol one at both aspects of subjective and objective assessment. High-b-value rFOV-syDWIs showed better image quality (overall image quality, anatomic details, lesion conspicuity, level of geometric deformation), SNR, and CNR than rFOV-sDWIs ($p < 0.05$). Histogram-derived syADC parameters except syADC$_{skewness}$ and syADC$_{kurtosis}$ showed significant differences to histogram-derived sADC parameters. Both 13b- and 5b-protocol syADC$_{mean}$ and syADC$_{minimum}$ showed higher diagnosis performance on cervical cancer than the resting histogram-derived 13b-protocol and 5b-protocol syADC parameters and the cutoffs of syADC$_{mean}$ and syADC$_{minimum}$ were almost the same for both multiple-b-value acquisition protocol. All indicated that synthetic high-b-value DWIs might be an alternative image for diagnosing cervical cancers with better lesion clarity and contrast as well as possess diagnostic performance equivalent to actually scanned DWIs; however, histogram-derived synthetic ADC parameters should be cautious when used to differentiate cervical cancer from normal tissues.

The diagnostic performance of high-b-value DWI on human organs such as brain and prostate is important in spite that it may be challenging to directly acquire high-b-value images [19, 20, 33, 34]. High-b-value images often show low SNR and CNR and serious eddy current distortion due to the on–off-switched diffusion gradient and long acquisition time that might thus degrade image quality. But, scanned high-b-value DWIs of cervical cancer showed better performance on grading tumor and more signal loss in the background [35]. Therefore, the concept of synthetic high-b-value DWI was desired in clinics to overcome these drawbacks and retain the advantages. The first study of the synthetic high-b-value DWIs was explored in prostate and metastatic prostate cancer [20]. In this study, the expected signal intensity of each image voxel for high-b-value synthetic DWIs was

Table 2 Inter-rater agreements on subjective assessment of 13b-protocol scanned and 5b-protocol synthetic rFOV-DWIs with *b* values of 1200 and 1500 s/mm^2

B value	Overall image quality				Anatomy				Lesion conspicuity				Geometric distortion			
	Reader1	Reader2	Kappa	*p* value	Reader1	Reader2	Kappa	*p* value	Reader1	Reader2	Kappa	*p* value	Reader1	Reader2	Kappa	*p* value
s_{13b}1200	1.58 ± 0.49	1.64 ± 0.48	**0.767****	***p* < 0.001**	1.64 ± 0.48	1.67 ± 0.47	**0.816****	***p* < 0.001**	1.61 ± 0.49	1.61 ± 0.49	**0.766****	***p* < 0.001**	1.61 ± 0.49	1.64 ± 0.48	**0.704****	***p* < 0.001**
Sy_{5b}1200	3.42 ± 0.50	3.43 ± 0.50	**0.882****	***p* < 0.001**	3.51 ± 0.50	3.54 ± 0.50	**0.935****	***p* < 0.001**	3.21 ± 0.50	3.21 ± 0.50	**0.878****	***p* < 0.001**	3.53 ± 0.50	3.50 ± 0.50	**0.833****	***p* < 0.001**
S_{13b}1500	1.64 ± 0.48	1.64 ± 0.48	**0.759****	***p* < 0.001**	1.60 ± 0.49	1.64 ± 0.48	**0.822****	***p* < 0.001**	1.58 ± 0.48	1.58 ± 0.49	**0.771****	***p* < 0.001**	1.58 ± 0.49	1.68 ± 0.47	**0.706****	***p* < 0.001**
Sy_{5b}1500	3.52 ± 0.49	3.54 ± 0.49	**0.885****	***p* < 0.001**	3.55 ± 0.49	3.57 ± 0.50	**0.936****	***p* < 0.001**	3.57 ± 0.49	3.57 ± 0.49	**0.885****	***p* < 0.001**	3.50 ± 0.50	3.56 ± 0.50	**0.830****	***p* < 0.001**

s = scanned DWI, sy = synthetic DWI, the image scores are expressed as means ± standard deviations, *p* values < 0.001 were considered statistically significant

**$p < 0.001$

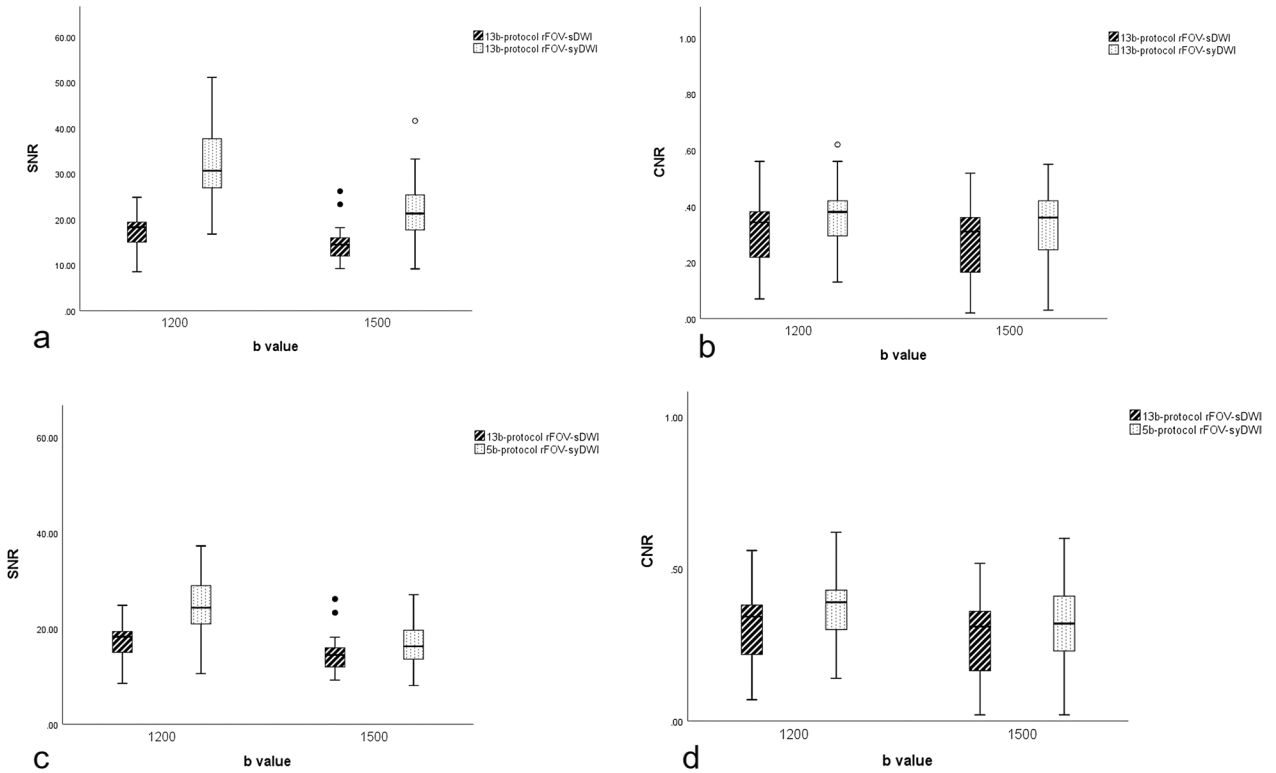

Fig. 2 Box plots illustrating the relationship between SNR (**a**) and CNR (**b**) of 13b-protocol scanned and synthetic rFOV-DWIs. And SNR (**c**), CNR (**d**) of 13b-protocol scanned and 5b-protocol synthetic rFOV-DWIs

extrapolated based on ADC maps computed using at least two low-b-value DWIs, indicating that computed high-b-value DWIs possess high SNR. In our study, four measurements in subjective evaluation of image quality (overall image quality, anatomic deformation degree, background suppression, and geometric deformation degree), two independent readers obtained higher Kappa scores on the 13b- and 5b-protocol than actual scanned DWI images with $b = 1200$ and 1500 s/mm^2 (Tables 1, 2). In accordance with a study of ovarian cancer and prostate [18, 36], four subjective quality scores (background suppression, distortion, artifact, and overall image quality score) of $sDWI_{b=1500}$ were higher than those of $sDWI_{b=1000}$. Synthetic high-b-value DWIs possess improved contrast between lesions and normal tissues compared to scanned ones due to an image itself computed from low-b-value DWIs with higher SNR instead of averaging same high-b-value DWIs [37], thus slightly high CNR and increased detection rate of small lesions, pancreatic lesions, abdominal hollow organ tumors and cervical cancer [20, 21, 38]. However, scanned mammary gland DWIs demonstrated slightly higher CNR than synthetic DWIs [37] while scanned prostate DWIs showed no significant different CNR to synthetic ones. In our study, $syDWI_{b=1200}$ and $syDWI_{b=1500}$ showed slightly better CNR than scanned ones, partly explained for synthetic DWIs using a reduced field-of-view DWI sequence decrease magnetic inhomogeneity and dephasing-induced distortion [39]. Briefly, synthetic high-b-value DWI can highlight the tumor characteristics with higher SNR and CNR and equivalent diagnostic performance to actually scanned DWI. In addition, a combination of high-b-value DWI and T2-weighted imaging (T2WI) has been validated for improved diagnostic performance on cervical stromal invasion and the diagnostic specificity for detection of locally residual cervical tumors compared to the utility of T2WI alone [40, 41]. Therefore, rFOV-syDWIs in diagnosing cervical cancer are highly feasible in clinics.

Numerous studies have adopted ADC values in the prognosis of cervical cancer [42]; however, only some studies reported histogram-derived ADC maps in cervical cancer. An ADC value is influenced by molecular viscosity, membrane permeability, and cell structures, and histogram-derived parameters based on ADC values reflect cell heterogeneity in different physiological states. For example, the difference of ADC_{mean} values between pre- and post-concurrent chemoradiotherapy (CCRT)

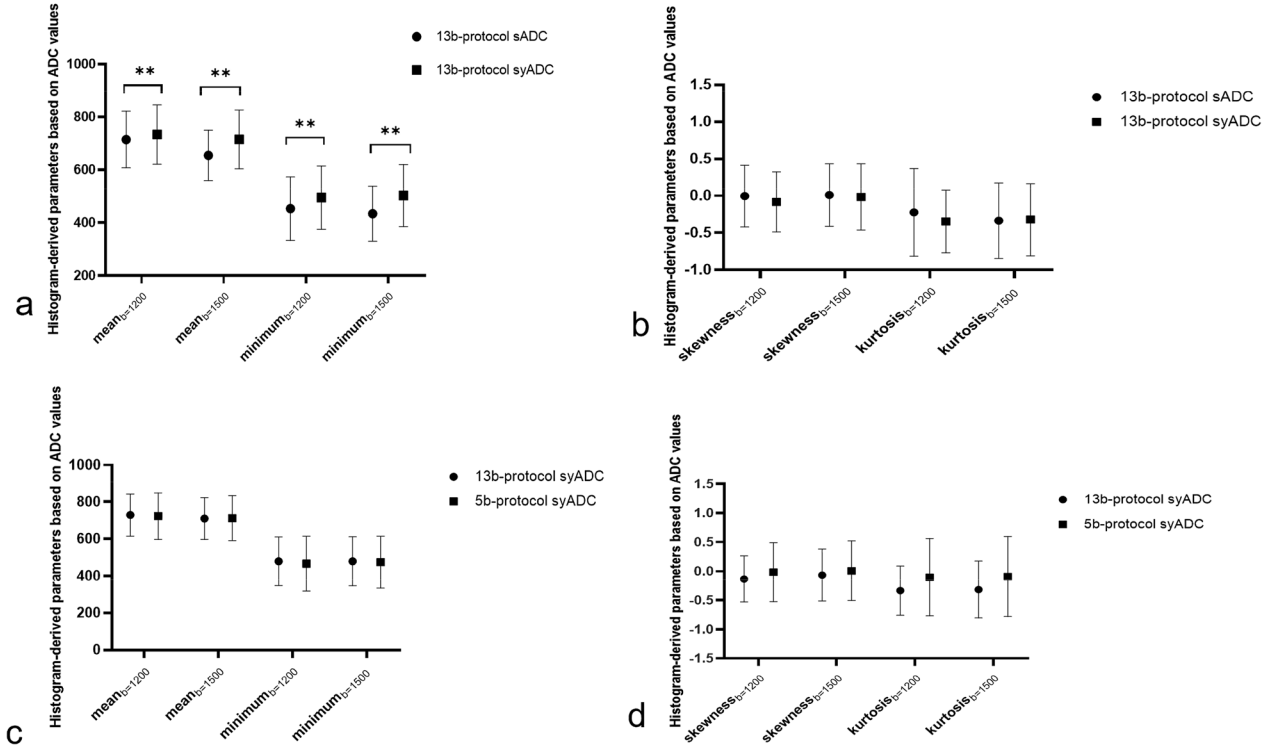

Fig. 3 Comparisons of histogram-derived parameters (mean minimum, skewness, and kurtosis): (**a, b**) based on 13b-protocol scanned and synthetic ADC values as well as those (**c, d**) based on 5b-protocol and 13b-protocol synthetic ADC values (**$p < 0.001$)

can predict the progression and survival of cervical cancer [43]; metastatic lymph nodes had a significantly lower $ADC_{minimum}$ than benign lymph nodes in endometrial cancer [14]. High-grade cervical cancer also has a significantly lower $ADC_{minimum}$ than low-grade cervical cancer [44]. Low ADC_{mean} and $ADC_{minimum}$ were attributed that high-density tumor cells and the narrowed extracellular space limit molecular diffusion in malignant tumors [45, 46]. Similar to the previous prostate study [14, 36], both 13b- and 5b-protocol $syADC_{mean}$ and $syADC_{minimum}$ showed good differentiation of cervical cancer from normal tissues and equivalent or even higher diagnostic performance than $sADC_{mean}$ and $sADC_{minimum}$ in our study. A true high-b-value ADC can be extrapolated with relatively small errors from the low-b-value DWIs due to the log-linear relationship between ADC and *b* values [38]; accordingly, $syADC_{mean}$ was equal to $sADC_{mean}$ and image quality scores of rFOV-syDWIs (subjective and objective image quality) were superior to those of rFOV-sDWIs in our study as previous studies [20, 21, 38]. Although histogram-derived parameters based on synthetic ADC values (except $ADC_{skewness}$ and $ADC_{kurtosis}$) of both lesion and control groups were statistically different to scanned ADC values ($p < 0.05$), the ROC curves of ADC_{mean} and $ADC_{minimum}$ but not $ADC_{kewness}$ and $ADC_{kurtosis}$ achieved the consistent diagnostic performance. Therefore, our study proved that $syADC_{mean}$ and $syADC_{minimum}$ can distinguish benign and malignant cervical lesions with extremely high diagnostic efficacy as $sADC_{mean}$ and $sADC_{minimum}$, and both may also play a role in prognosis such as predicting the disease progression and survival of patients with cervical cancer in the future. On the other hand, $ADC_{skewness}$ and $ADC_{kurtosis}$ had low diagnostic power probably due to the absence of hemorrhagic, necrotic, or cystic areas within the delineated ROIs in our study in spite that the presence of these excluding areas is considered to be an indicator of tumor heterogeneity [47]. A cervical cancer study showed $ADC_{skewness}$ and $ADC_{kurtosis}$ as well as the risk of lymph node metastasis elevates when the area with low ADC values (high cell density) increases [48]. A study of squamous cell carcinoma indicated that $ADC_{kurtosis}$ reduces as a steep peak turns into a wider and flatter peak when tumors become inhomogeneous [49]. Primary tumors with higher $ADC_{skewness}$ and $ADC_{kurtosis}$ easily fail in chemotherapy. $ADC_{skewness}$ and $ADC_{kurtosis}$ are knees to increase as cell death induces tumor heterogeneity. Therefore, no effective power of $ADC_{skewness}$ and $ADC_{kurtosis}$ was found in our study but they still have the potential in distinguishing malignant pelvic tumors

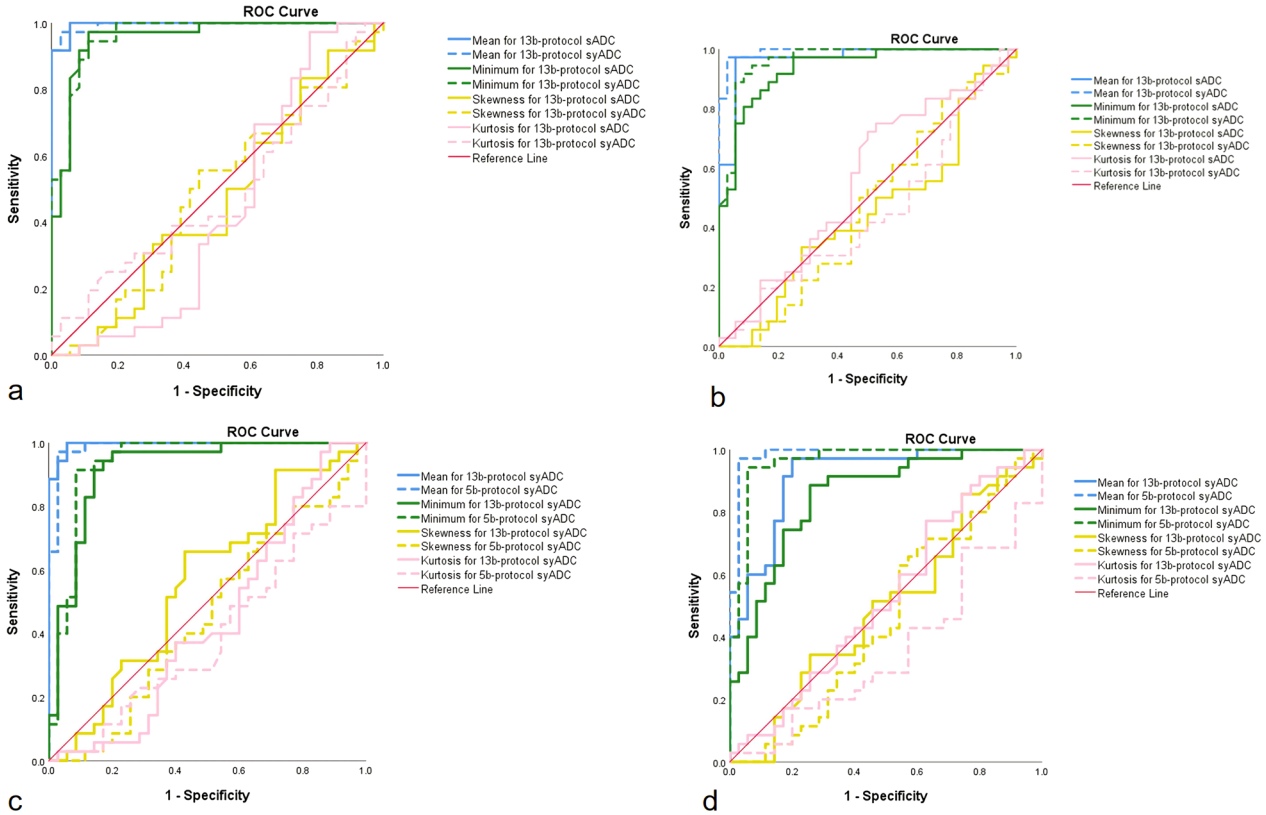

Fig. 4 Diagnosis efficiency of scanned and synthetic 13b-protocol ADC values with a *b* value of 0 and 1200 (**a**) or 1500 (**b**) s/mm^2 as well as that of synthetic 13b-protocol and 5b-protocol ADC values with a *b* value of 0 and 1200 (**c**) or 1500 (**d**) s/mm^2

Table 3 Diagnosis performance on cervical cancer of histogram-derived scanned and synthetic 13b-protocol ADC values with a *b* value of 0 and 1200 s/mm^2

Parameters	AUC (95%CI)	Sensitivity (%)	Specificity (%)	*p* value	Threshold (s/mm^2)
$sADC_{13b,mean}$	0.995 (0.987–1.000)	100.0	94.4	***p* < 0.05**	0.903×10^{-3}
$syADC_{13b,mean}$	0.995 (0.985–1.000)	97.2	97.2	***p* < 0.05**	0.941×10^{-3}
$sADC_{13b,minimum}$	0.956 (0.716–0.909)	91.7	88.9	***p* < 0.05**	0.573×10^{-3}
$syADC_{13b,minimum}$	0.961 (0.921–1.000)	94.4	88.9	***p* < 0.05**	0.633×10^{-3}
$sADC_{13b,skewness}$	0.463 (0.328–0.598)	91.7	16.7	$p = 0.33$	−0.515
$syADC_{13b,skewness}$	0.485 (0.349–0.620)	55.6	55.6	$p = 0.34$	−0.067
$sADC_{13b,kurtosis}$	0.439 (0.300–0.579)	97.2	22.2	$p = 0.30$	−0.793
$syADC_{13b,kurtosis}$	0.485 (0.349–0.621)	11.1	97.2	$p = 0.35$	−0.564

p values < 0.05 were considered statistically significant and are shown in bolded font

AUC = area under the receiver operating characteristic curve, 95%CI = 95% confidence intervals, sADC = scanned apparent diffusion coefficient, syADC = synthetic apparent diffusion coefficient

from benign ones in the future. Overall, the above-mentioned findings encouraged our team and also gave a hint to readers to observe the variance of histogram-derived ADC values in future clinical diagnosis, treatment response, and progress of cervical cancer, and assist decisions on radical hysterectomy or simple hysterectomy.

There are few limitations in our study. First, our study cohort and diversity were relatively small and this study was carried out in only one single institution. The study included patients with cervical squamous cell carcinoma but not with adenocarcinoma and small cell carcinoma. Therefore, our study results might not be

Table 4 Diagnosis performance on cervical cancer of histogram-derived scanned and synthetic 13b-protocol ADC values with a *b* value of 0 and 1500 s/mm^2

Parameters	AUC (95%CI)	Sensitivity (%)	Specificity (%)	*p* value	Threshold (s/mm^2)
$sADC_{13b,mean}$	0.968 (0.931–1.000)	97.2	94.4	**$p<0.05$**	0.789×10^{-3}
$syADC_{13b,mean}$	0.992 (0.979–1.000)	97.2	97.2	**$p<0.05$**	0.923×10^{-3}
$sADC_{13b,minimum}$	0.936 (0.883–0.989)	91.7	80.6	**$p<0.05$**	0.532×10^{-3}
$syADC_{13b,minimum}$	0.963 (0.923–1.000)	91.7	91.7	**$p<0.05$**	0.672×10^{-3}
$sADC_{13b,skewness}$	0.446 (0.311–0.580)	91.7	13.9	$p=0.31$	−0.542
$syADC_{13b,skewness}$	0.465 (0.349–0.620)	86.1	22.2	$p=0.03$	−0.393
$sADC_{13b,kurtosis}$	0.559 (0.424–0.693)	75.0	50.0	$p=0.42$	−0.529
$syADC_{13b,kurtosis}$	0.451 (0.317–0.586)	100	5.6	$p=0.32$	−0.986

p values < 0.05 were considered statistically significant and are shown in bolded font

AUC = area under the receiver operating characteristic curve, 95%CI = 95% confidence intervals, sADC = scanned apparent diffusion coefficient, syADC = synthetic apparent diffusion coefficient

Table 5 Diagnosis performance on cervical cancer of histogram-derived synthetic 13b-protocol and 5b-protocol ADC values with a *b* value of 0 and 1200 s/mm^2

Parameters	AUC (95%CI)	Sensitivity (%)	Specificity (%)	*p* value	Threshold(s/mm^2)
$syADC_{13b,mean}$	0.995 (0.985–1.000)	97.2	97.2	**$p<0.05$**	0.941×10^{-3}
$syADC_{5b,mean}$	0.988 (0.967–1.000)	97.1	97.1	**$p<0.05$**	0.934×10^{-3}
$syADC_{13b,minimum}$	0.961 (0.921–0.989)	94.4	88.9	**$p<0.05$**	0.633×10^{-3}
$syADC_{5b,minimum}$	0.935 (0.869–1.000)	91.4	91.4	**$p<0.05$**	0.654×10^{-3}
$syADC_{13b,skewness}$	0.485 (0.349–0.620)	55.6	55.6	$p=0.34$	−0.067
$syADC_{5b,skewness}$	0.452 (0.316–0.588)	8.6	74.3	$p=0.07$	−0.239
$syADC_{13b,kurtosis}$	0.485 (0.349–0.621)	11.1	97.2	$p=0.35$	−0.564
$syADC_{5b,kurtosis}$	0.387 (0.255–0.518)	28.6	48.6	$p=0.07$	−0.520

p values < 0.05 were considered statistically significant and are shown in bolded font

AUC = area under the receiver operating characteristic curve, 95%CI = 95% confidence intervals, syADC = synthetic apparent diffusion coefficient

Table 6 Diagnosis performance on cervical cancer of histogram-derived synthetic 13b-protocol and 5b-protocol ADC values with a b value of 0 and 1500 s/mm^2

Parameters	AUC (95%CI)	Sensitivity (%)	Specificity (%)	*p* value	Threshold (s/mm^2)
$syADC_{13b,mean}$	0.992 (0.979–1.000)	97.2	97.2	**$p<0.05$**	0.923×10^{-3}
$syADC_{5b,mean}$	0.984 (0.958–1.000)	97.1	97.1	**$p<0.05$**	0.910×10^{-3}
$syADC_{13b,minimum}$	0.963 (0.923–1.000)	91.7	91.7	**$p<0.05$**	0.672×10^{-3}
$syADC_{5b,minimum}$	0.962 (0.917–1.000)	94.3	94.3	**$p<0.05$**	0.645×10^{-3}
$syADC_{13b,skewness}$	0.465 (0.349–0.620)	86.1	22.2	$p=0.33$	−0.393
$syADC_{5b,skewness}$	0.460 (0.322–0.597)	11.4	71.4	$p=0.07$	−0.242
$syADC_{13b,kurtosis}$	0.451 (0.317–0.586)	100	5.6	$p=0.32$	−0.986
$syADC_{5b,kurtosis}$	0.355 (0.255–0.485)	45.7	25.7	$p=0.07$	−0.522

p values < 0.05 were considered statistically significant and are shown in bolded font

AUC = area under the receiver operating characteristic curve, 95%CI = 95% confidence intervals, syADC = synthetic apparent diffusion coefficient

generalized in all cervical diseases. Secondly, synthetic high-b-value images were conducted only on 1.5 T MRI. Direct comparison of computed DWI between different magnetic fields might be impractical and should be verified especially ADC values in disease diagnosis in spite that there is no significant difference in ADC values between cervical cancer and abdominal organs between 1.5 and 3.0 T [50]. It was worth noting that the exclusion of lesions smaller than 10 mm in our study increases the accuracy of ADC values but may lead to

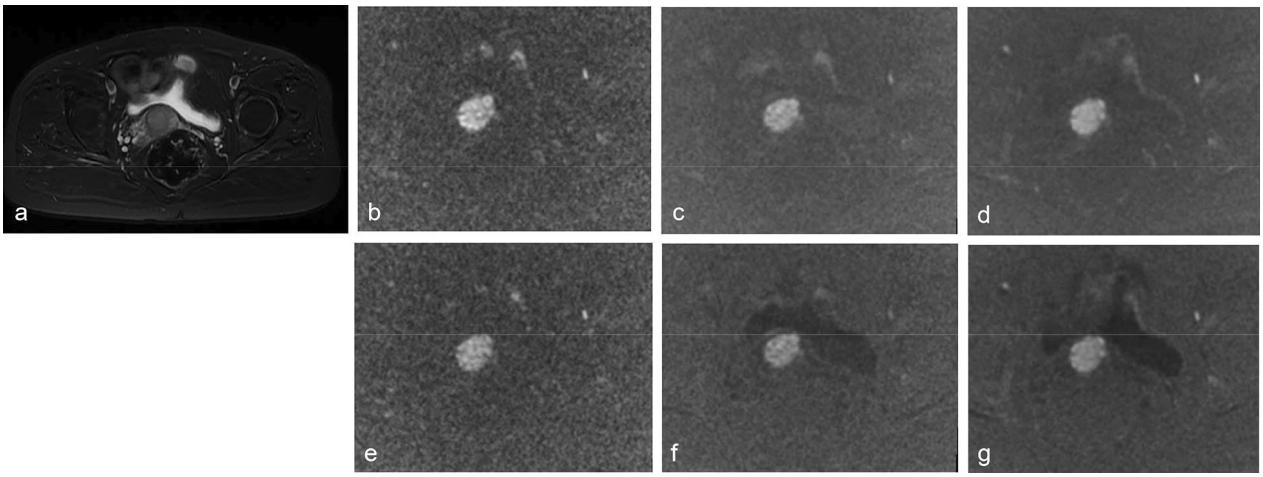

Fig. 5 A 65-year-old woman with stage IIB cervical cancer. Illustration of the significant lesions on T2-weighted image (**a)** as well as 13b-protocol and 5b-protocol rFOV-DWI with b value of 0 and 1200 or 1500 s/mm^2, including rFOV-sDWI$_{13b=1200}$ (**b**), rFOV-sDWI$_{13b=1500}$ (**e**), rFOV-syDWI$_{13b=1200}$ (**c**), rFOV-syDWI$_{13b=1500}$ (**f**), rFOV-syDWI$_{5b=1200}$ (**d**), and rFOV-syDWI$_{5b=1500}$ s/mm^2 (**g**)

bias in case selection. As in previous cervical studies, the maximum cross-sectional area was used to sketch lesion ROIs and areas such as hemorrhages, necrosis, or cysts were excluded so that target ROIs showed not much heterogeneous and led to lower differentiation power. More different pathological subtypes and delineation approaches should be explored in the future to conduct a large cohort study.

In conclusion, both 5b- and 13b-protocol generated rFOV-syDWIs with better lesion contrast and higher image quality and synthetic ADC values with equivalent diagnostic power to 13b-protocol scanned ones could be applied in the diagnosis of cervical cancer, whereas synthetic ADC values should be concerned when being used to differentiation of cervical squamous cell carcinoma from benign tumors. Moreover, 5b-protocol synthetic DWIs shorten scan time and synthetic ADCs offer reliable diagnosis value for reference. Of importance, good diagnostic performance of both ADC_{mean} and $ADC_{minimum}$ obtained using both synthetic and scanned DWIs showed reduced field-of-view DWI is reliable to be applied in clinics.

Abbreviations

$ADC_{kurtosis}$	Kurtosis of the apparent diffusion coefficient
$ADC_{maximum}$	Maximum apparent diffusion coefficient
ADC_{mean}	Mean apparent diffusion coefficient
$ADC_{minimum}$	Minimum apparent diffusion coefficient
$ADC_{skewness}$	Skewness of the apparent diffusion coefficient
CNR	Contrast-to-noise ratio
DWI	Diffusion-weighted imaging
f-FOV	Full field of view
rFOV	Reduced field of view
rFOV-DWI	Reduced full-of-view diffusion-weighted imaging
rFOV-sDWI	Scanned reduced full-of-view diffusion-weighted imaging
rFOV-syDWI	Synthetic reduced full-of-view diffusion-weighted imaging
sADC	Scanned apparent diffusion coefficient
sDWI	Scanned diffusion-weighted imaging
SNR	Signal-to-noise ratio
syADC	Synthetic apparent diffusion coefficient

Author contributions

QT participated in the topic selection and design of this study, analyzed and explained the feasibility and significance of uterine tumors reducing the synthesis of high-b-value diffusion-weighted imaging in the full field of view, and was a major contributor to the writing of this manuscript. QQZ participated in the topic selection and design, and LS, YX, and CL conducted relevant MRI sequence examinations and scans for the enrolled patients and volunteers in this study. WC made key modifications to the important aspects of his academic content, and LX and WVL reviewed and checked the final version of the paper and finally agreed to publish it. Finally, all authors read and approved the final draft and agreed to be responsible for the integrity of all aspects of the research work.

Availability of data and materials

The datasets generated and/or analyzed during the current study are not publicly available but are available from the corresponding author upon reasonable request.

Declarations

Ethics approval and consent to participate

This study has been approved by the Ethics Review Committee of Taihe Hospital, Shiyan City (IRB: 2022KS013), and all patients and volunteers in the study have signed written informed consent.

Consent for publication

All manuscript content in this study that contains details, images, etc., relevant to the individual has received informed written consent from the individual.

Competing interests

One of the authors (Weiyin Vivian Liu) is an employee of GE Healthcare. The remaining authors declare no competing interests.

Author details
[1]Department of Radiology, Taihe Hospital, Hubei University of Medicine, Shiyan, Hubei, China. [2]Biomedical Engineering College, Taihe Hospital, Hubei University of Medicine, Shiyan, Hubei, China. [3]GE Healthcare, Beijing, China.

Received: 12 June 2022 Accepted: 5 December 2022
Published online: 16 January 2023

References

1. Koh DM, Collins DJ (2007) Diffusion-weighted MRI in the body: applications and challenges in oncology. AJR Am J Roentgenol 188(6):1622–1635. https://doi.org/10.2214/AJR.06.1403
2. Blazic IM, Lilic GB, Gajic MM (2017) Quantitative assessment of rectal cancer response to neoadjuvant combined chemotherapy and radiation therapy: comparison of three methods of Positioning region of interest for ADC measurements at diffusion-weighted MR imaging. Radiology 282(2):418–428. https://doi.org/10.1148/radiol.2016151908
3. Naganawa S, Sato C, Kumada H et al (2005) Apparent diffusion coefficient in cervical cancer of the uterus: comparison with the normal uterine cervix. Eur Radiol 15(1):71–78. https://doi.org/10.1007/s00330-004-2529-4
4. Beddy P, Moyle P, Kataoka M et al (2012) Evaluation of depth of myometrial invasion and overall staging in endometrial cancer: comparison of diffusion-weighted and dynamic contrast-enhanced MR imaging. Radiology 262(2):530–537. https://doi.org/10.1148/radiol.11110984
5. Arita Y, Yoshida S, Waseda Y et al (2021) Diagnostic value of computed high b-value whole-body diffusion-weighted imaging for primary prostate cancer. Eur J Radiol 137:109581. https://doi.org/10.1016/j.ejrad.2021.109581
6. Zhang Z, Huang F, Ma X et al (2015) Self-feeding MUSE: a robust method for high resolution diffusion imaging using interleaved EPI. Neuroimage 105:552–560. https://doi.org/10.1016/j.neuroimage.2014.10.022
7. Saritas EU, Cunningham CH, Lee JH et al (2008) DWI of the spinal cord with reduced FOV single-shot EPI. Magn Reson Med 60(2):468–473. https://doi.org/10.1002/mrm.21640
8. Zaharchuk G, Saritas EU, Andre JB et al (2011) Reduced field-of-view diffusion imaging of the human spinal cord: comparison with conventional single-shot echo-planar imaging. AJNR Am J Neuroradiol 32(5):813–820. https://doi.org/10.3174/ajnr.A2418
9. Attenberger UI, Rathmann N, Sertdemir M et al (2016) Small Field-of-view single-shot EPI-DWI of the prostate: evaluation of spatially-tailored two-dimensional radiofrequency excitation pulses. Z Med Phys 26(2):168–176. https://doi.org/10.1016/j.zemedi.2015.06.013
10. Wu S, Zou X, Wang Q et al (2020) Gallbladder carcinoma: an initial clinical experience of reduced field-of-view diffusion-weighted MRI. Cancer Imaging 20(1):50. https://doi.org/10.1186/s40644-020-00326-x
11. Harder FN, Jung E, McTavish S et al (2022) High-resolution, High b-value computed diffusion-weighted imaging improves detection of pancreatic ductal adenocarcinoma. Cancers 14(3):470. https://doi.org/10.3390/cancers14030470
12. Chen M, Feng C, Wang Q et al (2021) Comparison of reduced field-of-view diffusion-weighted imaging (DWI) and conventional DWI techniques in the assessment of Cervical carcinoma at 3.0T: Image quality and FIGO staging. Eur J Radiol 137:109557. https://doi.org/10.1016/j.ejrad.2021.109557
13. Lemke A, Stieltjes B, Schad LR et al (2011) Toward an optimal distribution of b values for intravoxel incoherent motion imaging. Magn Reson Imaging 29(6):766–776. https://doi.org/10.1016/j.mri.2011.03.004
14. Jendoubi S, Wagner M, Montagne S et al (2019) MRI for prostate cancer: can computed high b-value DWI replace native acquisitions? Eur Radiol 29(10):5197–5204. https://doi.org/10.1007/s00330-019-06085-z
15. Ohlmeyer S, Laun FB, Bickelhaupt S et al (2021) Ultra-high b-value diffusion-weighted imaging-based abbreviated protocols for breast cancer detection. Invest Radiol 56(10):629–636. https://doi.org/10.1097/RLI.0000000000000784
16. Dietrich O, Biffar A, Baur-Melnyk A et al (2010) Technical aspects of MR diffusion imaging of the body. Eur J Radiol 76(3):314–322. https://doi.org/10.1016/j.ejrad.2010.02.018
17. Ichikawa T, Erturk SM, Motosugi U et al (2006) High-B-value diffusion-weighted MRI in colorectal cancer. AJR Am J Roentgenol 187(1):181–184. https://doi.org/10.2214/AJR.05.1005
18. Takeuchi M, Matsuzaki K, Harada M (2016) Computed diffusion-weighted imaging for differentiating decidualized endometrioma from ovarian cancer. Eur J Radiol 85(5):1016–1019. https://doi.org/10.1016/j.ejrad.2016.03.009
19. Le Bihan D, Poupon C, Amadon A, Lethimonnier F (2006) Artifacts and pitfalls in diffusion MRI. J Magn Reson Imaging 24(3):478–488. https://doi.org/10.1002/jmri.20683
20. Blackledge MD, Leach MO, Collins DJ et al (2010) Computed diffusion-weighted MR imaging may improve tumor detection. Radiology 261(2):573–581. https://doi.org/10.1148/radiol.11101919
21. Ortendahl DA, Hylton NM, Kaufman L et al (1984) Signal to noise in derived NMR images. Magn Reson Med 1(3):316–338. https://doi.org/10.1002/mrm.1910010304
22. Maas MC, Fütterer JJ, Scheenen TW et al (2013) Quantitative evaluation of computed high B value diffusion-weighted magnetic resonance imaging of the prostate. Invest Radiol 48(11):779–786. https://doi.org/10.1097/RLI.0b013e31829705bb
23. Sanderink WBG, Teuwen J, Appelman L et al (2021) Diffusion weighted imaging for evaluation of breast lesions: comparison between high b-value single-shot and routine readout-segmented sequences at 3 T. Magn Reson Imaging 84:35–40. https://doi.org/10.1016/j.mri.2021.09.007
24. Kawahara S, Isoda H, Fujimoto K et al (2016) Additional benefit of computed diffusion-weighted imaging for detection of hepatic metastases at 1.5T. Clin Imaging 40(3):481–485. https://doi.org/10.1016/j.clinimag.2015.12.007
25. Ichikawa S, Kromrey ML, Motosugi U et al (2021) Optimal target b-value on computed diffusion-weighted magnetic resonance imaging for visualization of pancreatic ductal adenocarcinoma and focal autoimmune pancreatitis. Abdom Radiol (NY) 46(2):636–646. https://doi.org/10.1007/s00261-020-02695-0
26. Ablefoni M, Surup H, Ehrengut C et al (2021) Diagnostic benefit of high b-value computed diffusion-weighted imaging in patients with hepatic metastasis. J Clin Med 10(22):5289. https://doi.org/10.3390/jcm10225289
27. Kitazume Y, Tsuchiya J, Takenaka K et al (2020) High b-value computed diffusion-weighted imaging for differentiating bowel inflammation in Crohn's disease. Eur J Radiol 133:109362. https://doi.org/10.1016/j.ejrad.2020.109362
28. Bhatla N, Berek JS, Cuello Fredes M et al (2019) Revised FIGO staging for carcinoma of the cervix uteri. Int J Gynaecol Obstet 45(1):129–135. https://doi.org/10.1002/ijgo.12749
29. Perucho JAU, Wang M, Vardhanabhuti V et al (2021) Association between IVIM parameters and treatment response in locally advanced squamous cell cervical cancer treated by chemoradiotherapy. Eur Radiol 31(10):7845–7854. https://doi.org/10.1007/s00330-021-07817-w
30. Zhang Q, Ouyang H, Ye F et al (2021) Feasibility of intravoxel incoherent motion diffusion-weighted imaging in distinguishing adenocarcinoma originated from uterine corpus or cervix. Abdom Radiol (NY) 46(2):732–744. https://doi.org/10.1007/s00261-020-02586-4
31. Hoogendam JP, Klerkx WM, de Kort GA et al (2010) The influence of the b-value combination on apparent diffusion coefficient based differentiation between malignant and benign tissue in cervical cancer. J Magn Reson Imaging 32(2):376–382. https://doi.org/10.1002/jmri.22236
32. Padhani AR, Liu G, Koh DM et al (2009) Diffusion-weighted magnetic resonance imaging as a cancer biomarker: consensus and recommendations. Neoplasia 11(2):102–125. https://doi.org/10.1593/neo.81328
33. Katahira K, Takahara T, Kwee TC et al (2011) Ultra-high-b-value diffusion-weighted MR imaging for the detection of prostate cancer: evaluation in 201 cases with histopathological correlation. Eur Radiol 21(1):188–196. https://doi.org/10.1007/s00330-010-1883-7
34. Cihangiroglu M, Uluğ AM, Firat Z et al (2009) High b-value diffusion-weighted MR imaging of normal brain at 3T. Eur J Radiol 69(3):454–458. https://doi.org/10.1016/j.ejrad.2007.11.023
35. Qi YF, He YL, Lin CY et al (2020) Diffusion-weighted imaging of cervical cancer: feasibility of ultra-high b-value at 3T. Eur J Radiol 124:108779. https://doi.org/10.1016/j.ejrad.2019.108779

36. Rosenkrantz AB, Chandarana H, Hindman N et al (2013) Computed diffusion-weighted imaging of the prostate at 3 T: impact on image quality and tumour detection. Eur Radiol 23(11):3170–3177. https://doi.org/10.1007/s00330-013-2917-8
37. DelPriore MR, Biswas D, Hippe DS et al (2021) Breast cancer conspicuity on computed versus acquired high b-value diffusion-weighted MRI. Acad Radiol 28(8):1108–1117. https://doi.org/10.1016/j.acra.2020.03.011
38. Sahoo P, Rockne RC, Jung A et al (2020) Synthetic apparent diffusion coefficient for high b-value diffusion-weighted MRI in prostate. Prostate Cancer 2020:5091218. https://doi.org/10.1155/2020/5091218
39. Harder FN, Kamal O, Kaissis GA et al (2021) Qualitative and quantitative comparison of respiratory triggered reduced field-of-view (FOV) versus full FOV diffusion weighted imaging (DWI) in pancreatic pathologies. Acad Radiol 28(Suppl 1):S234–S243. https://doi.org/10.1016/j.acra.2020.12.011
40. Park JJ, Kim CK, Park SY et al (2015) Parametrial invasion in cervical cancer: fused T2-weighted imaging and high-b-value diffusion-weighted imaging with background body signal suppression at 3 T. Radiology 274(3):734–741. https://doi.org/10.1148/radiol.14140920
41. Thomeer MG, Vandecaveye V, Braun L et al (2019) Evaluation of T2-W MR imaging and diffusion-weighted imaging for the early post-treatment local response assessment of patients treated conservatively for cervical cancer: a multicentre study. Eur Radiol 29(1):309–318. https://doi.org/10.1007/s00330-018-5510-3
42. Harry VN, Persad S, Bassaw B et al (2021) Diffusion-weighted MRI to detect early response to chemoradiation in cervical cancer: a systematic review and meta-analysis. Gynecol Oncol Rep 38:100883. https://doi.org/10.1016/j.gore.2021.100883
43. Gu KW, Kim CK, Choi CH et al (2019) Prognostic value of ADC quantification for clinical outcome in uterine cervical cancer treated with concurrent chemoradiotherapy. Eur Radiol 29(11):6236–6244. https://doi.org/10.1007/s00330-019-06204-w
44. Schob S, Meyer HJ, Pazaitis N et al (2017) ADC histogram analysis of cervical cancer aids detecting lymphatic Metastases-a preliminary study. Mol Imaging Biol 19(6):953–962. https://doi.org/10.1007/s11307-017-1073-y
45. Rechichi G, Galimberti S, Oriani M et al (2013) ADC maps in the prediction of pelvic lymph nodal metastatic regions in endometrial cancer. Eur Radiol 23(1):65–74. https://doi.org/10.1007/s00330-012-2575-2
46. Xue H, Ren C, Yang J et al (2014) Histogram analysis of apparent diffusion coefficient for the assessment of local aggressiveness of cervical cancer. Arch Gynecol Obstet 290(2):341–348. https://doi.org/10.1007/s00404-014-3221-9
47. Liu Y, Zhang Y, Cheng R et al (2019) Radiomics analysis of apparent diffusion coefficient in cervical cancer: a preliminary study on histological grade evaluation. J Magn Reson Imaging 49(1):280–290. https://doi.org/10.1002/jmri.26192
48. Becker AS, Ghafoor S, Marcon M et al (2017) MRI texture features may predict differentiation and nodal stage of cervical cancer: a pilot study. Acta Radiol Open 6(10):2058460117729574. https://doi.org/10.1177/2058460117729574
49. King AD, Chow KK, Yu KH et al (2013) Head and neck squamous cell carcinoma: diagnostic performance of diffusion-weighted MR imaging for the prediction of treatment response. Radiology 266(2):531–538. https://doi.org/10.1148/radiol.12120167
50. Rosenkrantz AB, Oei M, Babb JS et al (2011) Diffusion-weighted imaging of the abdomen at 3.0 Tesla: image quality and apparent diffusion coefficient reproducibility compared with 1.5 Tesla. J Magn Reson Imaging 33(1):128–135. https://doi.org/10.1002/jmri.22395

Publisher's Note